Research

CrossMark
click for updates

Author for correspondence:
Yu-Chie Chen
e-mail: yuchie@mail.nctu.edu.tw

Revisiting the quantitative features of surface-assisted laser desorption/ionization mass spectrometric analysis

Ching-Yi Wu, Kai-Chieh Lee, Yen-Ling Kuo and Yu-Chie Chen

Department of Applied Chemistry, National Chiao Tung University, Hsinchu 300, Taiwan

iD C-YW, 0000-0002-2598-7310; K-CL, 0000-0002-3485-099X; Y-LK, 0000-0003-2908-5311; Y-CC, 0000-0003-2253-4049

Surface-assisted laser desorption/ionization (SALDI) coupled with mass spectrometry (MS) is frequently used to analyse small organics owing to its clean background. Inorganic materials can be used as energy absorbers and the transfer medium to facilitate the desorption/ionization of analytes; thus, they are used as SALDI-assisting materials. Many studies have demonstrated the usefulness of SALDI-MS in quantitative analysis of small organics. However, some characteristics occurring in SALDI-MS require certain attention to ensure the reliability of the quantitative analysis results. The appearance of a coffee-ring effect in SALDI sample preparation is the primary factor that can affect quantitative SALDI-MS analysis results. However, to the best of our knowledge, there are no reports relating to quantitative SALDI-MS analysis that discuss or consider this effect. In this study, the coffee-ring effect is discussed using nanoparticles and nanostructured substrates as SALDI-assisting materials to show how this effect influences SALDI-MS analysis results. Potential solutions for overcoming the existing problems are also suggested.

This article is part of the themed issue 'Quantitative mass spectrometry'.

THE ROYAL SOCIETY PUBLISHING

1. Introduction

(a) Surface-assisted laser desorption/ionization–mass spectrometry

Matrix-assisted laser desorption/ionization (MALDI) coupled with mass spectrometry (MS) [1,2] is widely used to analyse various substances, such as peptides, proteins and polymers. Given the high-matrix background in the low-mass region [3], conventional MALDI-MS is seldom used as a detection tool for small molecules. Furthermore, poor shot-to-shot reproducibility also leads to MALDI-MS being unsuitable for quantitative analysis. Surface-assisted laser desorption/ionization (SALDI) coupled with MS (SALDI-MS) [4] has been considered as an alternative for the analysis of small molecules and for quantitative analysis owing to its unique features, including a low-matrix background and improved shot-to-shot reproducibility.

SALDI was first proposed and named by Sunner *et al.* in 1995 [4]. Contrary to MALDI, graphite powder was initially used as the energy-absorption medium to absorb laser light for assisting the desorption/ionization of analytes in SALDI. Furthermore, liquid glycerol was mixed with graphite powder to buffer the energy transfer and to provide a proton source for facilitating the desorption/ionization process. Therefore, the shot-to-shot reproducibility was improved because of the presence of liquid glycerol in the samples. Tanaka *et al.* [3] used a mixture of cobalt nanoparticles (NPs) combined with glycerol as the assisting substrate for the analysis of large proteins in laser desorption MS before SALDI was introduced. The work was mainly focused on the analysis of large biomolecules [3].

Although carbon materials such as graphite powder [4] and active carbon powder [5–7] are readily available, other types of inorganic materials [8–36] can also be used as SALDI-assisting materials. In particular, generating a variety of nanomaterials becomes an easy task owing to the progress of nanotechnology in the past few decades. Thus, different nanomaterials have been examined as SALDI-assisting materials to facilitate desorption/ionization of analytes in SALDI-MS [8–36]. Given the low-matrix background, most studies were focused on the application of SALDI-MS in the analysis of small molecules [16–36]. Furthermore, the possibility of using SALDI-MS for quantitative analysis was studied [16–36]. Although liquid glycerol was added to the samples to facilitate the desorption/ionization process, acid-containing or amine-containing salts such as citrate acid and ammonium citrate have also been used as alternatives [10,11,13]. Glycerol has a low vapour pressure but the requirement for high vacuum in the mass spectrometer does not allow the simultaneous introduction of numerous samples containing glycerol to a mass spectrometer. However, shot-to-shot reproducibility in the glycerol-containing SALDI materials is much better than when salts such as ammonium citrate and citric acid are used in SALDI. In general, the shot-to-shot reproducibility in SALDI-MS is better than that in MALDI-MS.

(b) Inorganic nanoparticles used in quantitative surface-assisted laser desorption/ionization–mass spectrometry analysis

The electronic supplementary material, table S1, lists a variety of inorganic particles that have been used in quantitative SALDI-MS analysis. Carbon materials including porous oxidized graphitized carbon black powder [16], multi-walled carbon nanotubes [17] and graphitic carbon nitride nanosheets [18], which possess an absorption capacity in the wide electromagnetic spectrum, have been used in the quantitative SALDI analysis of small drugs or small organics. Au NPs [19–24] are widely used in quantitative SALDI-MS analysis. In addition to ease of preparation and functionalization, Au NPs also possess a desirable absorption capacity in the ultraviolet (UV) region, which the wavelength of the laser used in SALDI-MS belongs to. This consideration is also one of the reasons why Au NPs are selected as SALDI-assisting materials. However, Au nanocluster ions, e.g. Au_n^+ ($n = 1, 2, 3$, etc.), generated from Au NPs are easily generated during SALDI-MS analysis [24]. Au NP-based SALDI-MS has been applied in the quantitative analysis

[19–24] of small organics, small biomolecules and drugs. The particle size of the Au NPs used in most of these studies is in the range of 10–20 nm [20–23]. Au NPs with particle sizes of less than 10 nm [19] and greater than 20 nm [24] used as SALDI-assisting materials have also reported. In addition, Ag NPs that have similar properties to Au NPs including a desirable absorption capacity in the UV region and ease of generation and functionalization have been used as SALDI-assisting materials in quantitative SALDI-MS [25,26]. The particle size of these Ag NPs was 10–30 nm. Ag NP-based SALDI-MS has been used in the quantitative analysis of small biomolecules [25,26]. Metal oxide NPs such as Fe_3O_4 magnetic NPs (MNPs) [27] and TiO_2 NPs [28–31] are also useful SALDI-assisting materials owing to their absorption capacity toward the laser light used in SALDI-MS. They also possess the feature of ease of surface functionalization. Thus, these metal oxide NPs work as suitable SALDI-assisting materials, and can be used as affinity probes to concentrate their target species prior to SALDI-MS analysis. Moreover, the magnetic properties of Fe_3O_4 MNPs allow easy implementation of the concentration steps. The numbers of ions generated from metal oxide NPs and that contribute to the background are usually much fewer than those from Au NPs and Ag NPs. HgTe nanostructured particles [32] and zinc sulfide particles [33] have also been used in the quantitative analysis of cyclodextrins. From the reports discussed above, if inorganic particles have the capacity to be used as energy absorbers in SALDI-MS and contribute only a few background ions in the SALDI mass spectra, they can be regarded as suitable SALDI-assisting materials.

The dynamic range in quantitative SALDI-MS analysis is generally from approximately 1 µM to approximately 100 µM, whereas the limit of detection is in the sub-micromolar range (electronic supplementary material, table S1). The linear correlation coefficients (R^2) are commonly reported to be as high as approximately 0.99 (electronic supplementary material, table S1). Thus, these studies generally concluded that satisfactory quantitative results were obtained using SALDI-MS as a detection tool. However, considering the characteristics of SALDI, the reliability of using SALDI-MS for quantitative analysis has to be revisited.

(c) Nanostructured films used in quantitative surface-assisted laser desorption/ionization– mass spectrometry analysis

Apart from the assisting materials with particle forms, a number of films with nanostructures that have the capability to assist quantitative SALDI-MS analysis have also been explored [34–36]. Silicon nanostructured films [34,35] are the most common substrates used in quantitative SALDI-MS analysis (electronic supplementary material, table S1). For example, silicon nanopillar arrays [34], desorption ionization on porous silicon [35] and nanostructured silicon substrates functionalized with fluorine-containing species [35] have been used as suitable SALDI-assisting materials for quantitative SALDI-MS analysis of drugs such as oxycodone [34,35]. Moreover, indium tin oxide coating substrates are useful SALDI-assisting materials for quantitative SALDI-MS analysis of lactose [36].

However, some problems such as the appearance of coffee-ring effects [37,38] have to be considered when conducting SALDI-MS for quantitative analysis and when using proton-rich salts as the proton source. This will be discussed further in the following sections.

2. Experimental

(a) Preparation of Au nanoparticles on a sample target

The details of the chemicals used in this study and the generation of Au NPs are described in the electronic supplementary material. The Au NP suspension (1 ml) was individually loaded into five centrifuge tubes, followed by centrifugation at 12 000 r.p.m. for 20 min. The supernatant (900 µl) from each tube was discarded. Aqueous trisodium citrates (4 mM) with volumes of 1900, 1233, 900, 700 and 566 µl were added individually to the five tubes. Thus, the final concentrations of the Au NPs in the five tubes were 7.50, 11.25, 15.00, 18.75 and 22.50 nM. The Au NP suspension

(0.5 µl) from each of the five tubes was deposited in the wells in a stainless sample target. After air drying, the deposits were photographed using a camera and a Nikon Eclipse 80i microscope (Tokyo, Japan) with a 10 × objective lens, a 10 × eyepiece lens, and an oil immersion condenser of 1.43–1.20 (Nikon) under dark field. The exposure time was set at 3 s.

(b) Preparation of surface-assisted laser desorption/ionization samples on the nanostructured film for mass spectrometric imaging

The details of the generation of titania nanotube arrays (TNAs) are given in the electronic supplementary material. The surface of the generated TNAs was hydrophilic. To limit the sample deposition to a confined area, we generated sample wells on the TNAs by adhering with a copper tape that contained spherical holes with a defined diameter. The spherical holes on the copper tape were created using a punch tool that could make spherical holes with a diameter of 1 mm. The resultant copper tape was then adhered to a TNA-based substrate that had been adhered to a sample plate. Finally, sample droplets were deposited on the holes in the TNA substrate to load the samples. Dodecyltrimethylammonium bromide (DeTAB) was selected as the analyte and decyltrimethyl ammonium bromide (DTAB) was used as the internal standard. DeTAB was prepared in deionized water at concentrations of 0.50, 1.00, 1.25, 2.50 and 5.00 µM. DTAB (1 µM) was also prepared in deionized water. Different concentrations of DeTAB (5 µl) were mixed with DTAB (5 µl and 1 µM). Then, the mixture (0.5 µl) was deposited on the TNA-based substrate, which was adhered to a stainless sample target. After air drying, the samples were introduced into a mass spectrometer for SALDI-MS analysis. Mass spectrometric imaging was carried out using an AutoFlex III MALDI mass spectrometer (Bruker Daltonics, Breman, Germany). FlexImaging software (v. 2.0; Bruker Daltonics) was used to treat the resultant data.

3. Results and discussion

(a) Coffee-ring effect

The sample deposition in most of the quantitative NP-based SALDI-MS analysis approaches was generally conducted by a so-called dried droplet method (electronic supplementary material, table S1). Namely, a sample and NPs were mixed first and then a microlitre-sized droplet was deposited on the sample target. After solvent evaporation, the samples were ready for SALDI-MS analysis. A 'coffee ring' [38] is commonly observed when depositing a droplet of particle suspension on a solid substrate followed by solvent evaporation. A ring-like deposit containing particles along the boundary appears after drying. The occurrence of this phenomenon cannot be avoided in the sample preparation for SALDI-MS analysis [37,39]. The appearance of analyte ion signals relies on the assistance of the NPs such as Au NPs, and, thus, examining the distribution of the SALDI-assisting materials is important. We used Au NPs as the example to show how a coffee ring derived from a droplet containing Au NP (approx. 13 nm) was formed on a stainless sample plate. Figure 1a shows the photographs obtained after depositing a droplet (approx. 0.5 µl) containing different concentrations of Au NPs on the wells of the sample plate. Although the background was dark, a ring composed of Au NPs appeared in each well. An oval-shaped coffee ring was observed owing to the anisotropic structure of the stainless sample target (figure 1a). Furthermore, the ring became thicker as the concentration of the Au NPs increased (left to right). Figure 1b shows the optical microscopic images obtained under dark field after depositing a droplet containing Au NPs with concentrations from low to high (left to right). The sample spots were incompletely covered by the Au NPs. When the concentration of the Au NPs was increased to 22.5 nM, a number of Au NPs could distribute within the ring. However, the distribution of the Au NPs was heterogeneous (figure 1b). The common concentration of the Au NPs used as the assisting materials in quantitative SALDI-MS was approximately 15 nM [20,22], which was in the concentration range shown in figure 1.
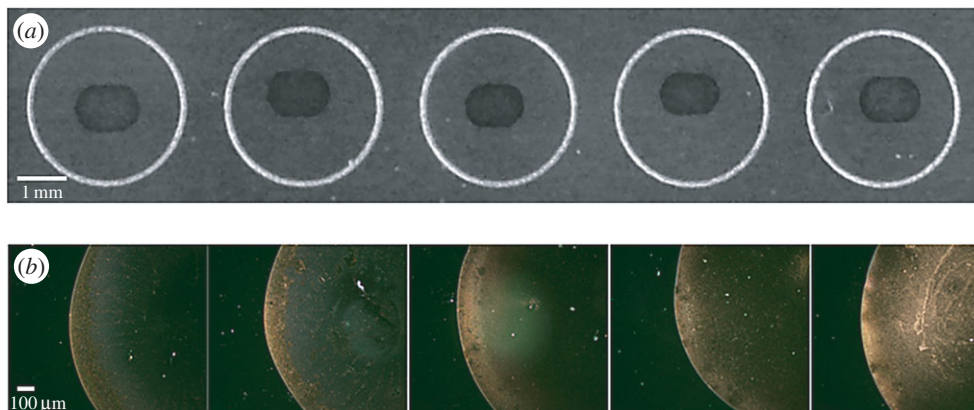
Figure 1. (*a*) The photographs obtained after depositing a droplet (approx. 0.5 μl) containing different concentrations of Au NPs on the wells of the sample plate and (*b*) their corresponding microscopic images obtained from dark field. The concentrations of the Au NPs from left to right were 7.50, 11.25, 15.00, 18.75 and 22.50 nM.

The results showed that heterogeneous Au NP deposition was formed when depositing a droplet containing Au NPs on the sample plate followed by solvent evaporation. Furthermore, the corresponding SALDI-MS image of the sample containing AuNPs (15 nM) also shows a ring when using the ion at *m/z* 215 as the target ion (electronic supplementary material, figure S1). The ion at *m/z* 215, i.e. the sodium adduct of citric acid, is derived from the ligand attached to the surface of the Au NPs. In addition, SALDI-assisting materials such as Au NPs contribute their Au cluster ions to background ions during SALDI-MS analysis. Therefore, the appearance of the intense background ions may easily suppress the appearance of the target analyte ions in the mass spectra.

A few solutions may be potentially used to suppress the coffee-ring effect in SALDI sample preparation. Most of the existing studies used a standard sample plate with non-hydrophobic properties to load with hydrophilic SALDI samples. Therefore, a coffee ring was easily formed during sample preparation. Heterogeneous sample deposition resulting from the coffee-ring effect could be expected although no reports related to quantitative SALDI-MS analysis have paid attention to this issue. Alternatively, the surface of the sample target can be modified to be hydrophobic to reduce the coffee-ring effect occurring in a hydrophilic sample droplet [37]. Notably, the data points were collected to obtain reliable quantitative SALDI-MS analysis results. Most of the existing studies stated how many sample spots in a sample were acquired. However, no reports have evaluated whether the coffee-ring effect has caused some bias in the data. In addition, when the Au cluster ions generated from Au NPs are used as background ions, analyte ion signals are suppressed by the presence of high-intensity Au cluster ions. The distribution of analytes on the SALDI-assisting materials would also affect the quantitative analysis results. Unfortunately, the coffee-ring effect can also affect the distribution of the analytes in a droplet after solvent evaporation. To eliminate the contribution of the coffee-ring effect by the SALDI-assisting materials, nanostructured films can be used as alternatives. The distribution of analytes on the SALDI-assisting materials can then be discussed solely. As mentioned earlier, using films as the SALDI-assisting materials is advantageous in that the distribution of SALDI-assisting materials can be ignored. The films are supposed to be homogeneous and can facilitate the desorption/ionization of analytes.

(b) Titania nanotube array-based quantitative surface-assisted laser desorption/ ionization–mass spectrometry analysis

TNAs have been used as suitable assisting materials in SALDI-MS analysis [13]. The assisting capability of TNAs was gained from their anatase crystallines because of their absorption capacity
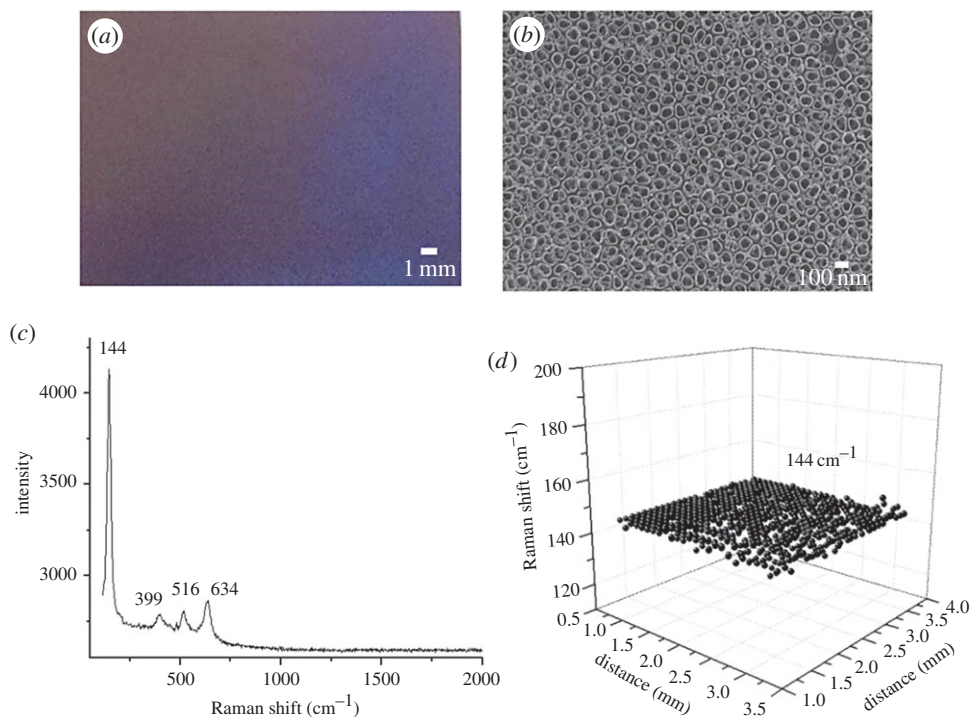
Figure 2. (*a*) Representative photograph of the generated TNAs. (*b*) Representative SEM image of the generated TNAs. (*c*) Representative Raman spectrum of the generated TNAs. (*d*) Raman spectral image of the TNAs by scanning the Raman shift at 144 cm^{-1}.

in the UV region [40]. When a TNA-based film is used as the SALDI-assisting material, the homogeneity of the anatase crystallines on the TNA film can be examined by Raman spectroscopy. Figure 2*a* shows a photograph of the generated TNAs, which have a metallic lustre and appear blueish. Figure 2*b* shows the image of the generated TNAs obtained from scanning electron microscopy (SEM). Titania nanotubes with an inner diameter of approximately 100 nm were observed. Figure 2*c* shows the representative Raman spectrum of the generated TNAs. The Raman peaks at 144, 399, 516 and 634 cm^{-1}, representing the characteristic peaks of the anatase crystalline [41], were observed. These peaks indicate the formation of anatase crystallines. Raman spectroscopic imaging was used to examine the entire area of the TNAs to ensure the homogeneity of anatase on the TNAs. The Raman shift at 144 cm^{-1} is the highest among these characteristic anatase peaks, and, thus, this peak was selected as the target to evaluate the distribution of anatase on the TNAs. Figure 2*d* shows the representative resultant Raman image of the TNA-based film by scanning the presence of the Raman shift at 144 cm^{-1}. The distribution of the Raman shift at 144 cm^{-1} on the TNAs was quite homogeneous.

After confirming the homogeneity of anatase crystallines on the generated TNAs, we further used the TNAs as the SALDI-assisting materials to load with samples. Small wells on the TNAs were prepared to restrain sample droplets to the limited area as described in the experimental section. Without using the sample well to restrict the sample deposition, the droplet was quickly spread out because of the highly hydrophilic surface of the TNAs (electronic supplementary material, figure S2). Electronic supplementary material, figure S3*a*, shows a water droplet deposited on the sample well, whereas figure S3*b* shows the photograph obtained after the droplet was dried. A droplet could remain on the well before drying. Namely, the coffee-ring effect and a large sample deposition area can be reduced using the designed sample wells. A cationic surfactant, i.e. DeTAB, was used as the analyte to simplify the discussion. DeTAB is a precharged analyte and thus adding a proton source in the sample is unnecessary. The
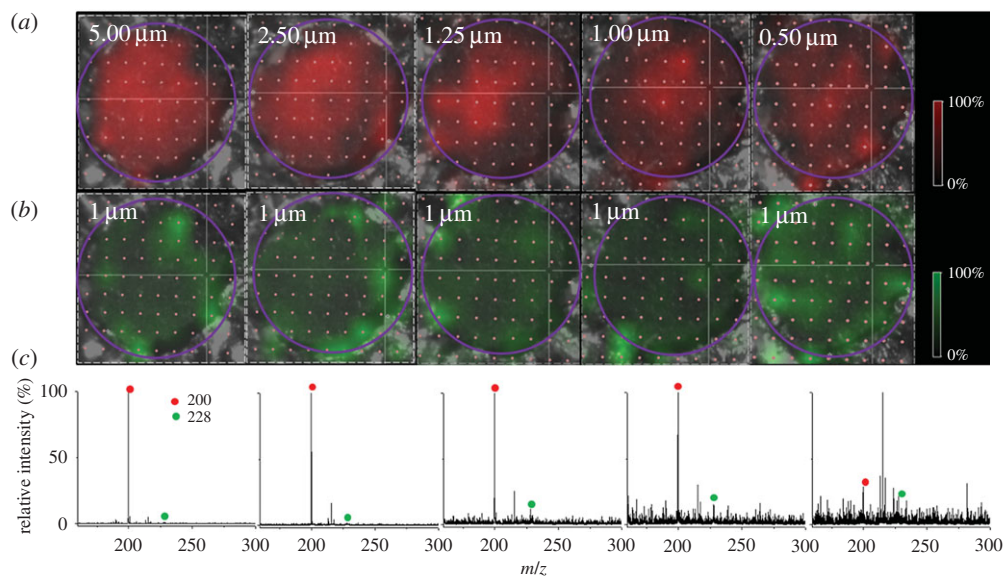
Figure 3. (*a*) Representative SALDI-MS images at *m/z* 200 derived from DeTAB, with the concentration range of 5.00, 2.50, 1.25, 1.00 and 0.50 μM (left to right). (*b*) Representative SALDI-MS images at *m/z* 228 derived from DTAB (1 μM). The purple circles indicate the area considered in the quantitative analysis. (*c*) The corresponding representative mass spectra derived from the same sample in the same column. The red circles indicate the peaks at *m/z* 200, while the green circles indicate the peaks at *m/z* 228.

contribution and effect caused by the proton source in the sample preparation can be ignored to simplify the discussion. Furthermore, the effect on the ionization efficiency can be disregarded. DTAB, which is in the same category of cationic surfactants as DeTAB, was also used as the internal standard (i.s.). To examine the ion distribution on the TNAs, SALDI-MS imaging was used for the investigation. Figure 3*a* shows the representative SALDI-MS images at *m/z* 200 derived from DeTAB, with a concentration range of 5.0–0.5 μM (left to right). Figure 3*b* shows the SALDI-MS image at *m/z* 228 derived from DTAB. Apparently, the intensity of the ion at *m/z* 200 decreased as the concentration of DeTAB decreased. The ion image at *m/z* 228 corresponding to DTAB was distributed in a roughly similar way in each image. Figure 3*c* shows the representative mass spectra obtained from the corresponding sample shown on the same column. The relative intensity of the ion peak *m/z* 200 decreased as the concentration of DeTAB decreased. Given that the sample droplet was restrained in the small well, the coffee-ring effect was insignificant. Nevertheless, the ion distribution in the SALDI images was inhomogeneous. Thus, the sum of the intensity-derived target analyte ions should be fully considered when considering the quantitative analysis.

Figure 4 shows the resultant calibration curve ($Y = -15.1 + 25.9X$, $R^2 = 0.994$) by plotting the ratio derived from the sum of the ion intensity at *m/z* 200 (DeTAB) to that of the ion intensity at *m/z* 228 (DTAB, i.s.) within the image versus the concentration of DeTAB within the sample deposition well. The ratios were obtained from three replicated experimental results. The linear regression coefficient was as high as 0.99. Nevertheless, it was apparent that a large error bar (more than 20%) was observed in each data point. The results show that it is possible to employ this approach for quantitative analysis. However, as the data varied quite a lot from different replicates, attention should be paid to avoiding personal bias. The results also indicate that the influence of the coffee-ring effect can be eliminated using proper sample preparation. Furthermore, all the intensity derived from the analyte ions within the sample deposition should be considered when conducting quantitative analysis to avoid any bias. The addition of an i.s. in the sample can also compensate for some uncertain operation or human errors.
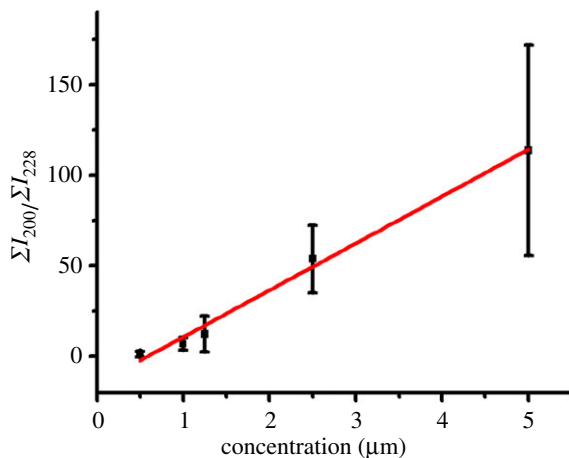
Figure 4. The resultant calibration curve based on the data obtained in figure 3. The curve was obtained by plotting the ratio of the sum of the total ion intensity at m/z 200 (ΣI_{200}) to that at m/z 228 (ΣI_{228}) versus the concentration of DeTAB. (Online version in colour.)

4. Conclusion

SALDI-MS is undoubtedly suitable for the analysis of small organics. However, some characteristics occurring in SALDI-MS sample preparation should be considered to obtain reliable quantitative analysis results. As discussed in this study, the coffee-ring effect seems to appear in the sample preparation when NPs are used as SALDI-assisting materials. Therefore, heterogeneous sample deposition can be expected. Further studies are required to explore suitable SALDI-assisting materials that may be able to suppress the coffee-ring effect. That is, if an aqueous NP suspension is deposited and used as the SALDI-assisting material, then the sample plate can be modified to be hydrophobic to prevent the generation of a coffee ring. Then, the entire sample deposit can be analysed and collected for quantitative SALDI-MS analysis. On the other hand, when using nanostructured films as the SALDI-assisting material, the coffee-ring effect can be reduced with a strategic sample preparation approach. When nanostructured-based film is used as the SALDI-assisting material, the use of a SALDI-MS image to acquire the data from the entire sample deposit to avoid any bias is suggested. The film should have homogeneous-assisting capacity through the entire film surface. A good linearity was obtained in the selected dynamic range, while the variation was large in each data point as observed in the calibration curve. Although all the existing reports have stated that good linearity in a certain dynamic concentration range can be obtained in their calibration curves, one should pay attention to how the data point is sampled to prevent any possibility of reaching incorrect conclusions. In addition, the use of NPs may cause some problems during laser irradiation. NPs can be easily sputtered during laser irradiation, leading to possible contamination of the ion source. One should be cautious and prevent any damage to the turbo pump when using NPs as SALDI-assisting materials. On the other hand, this concern can be eliminated using nanostructured films as the assisting materials in quantitative SALDI-MS analysis. In addition, the results may be further improved by using an extremely small sample volume (approx. picolitres) and small deposition spot (approx. 100 µm) [42]. Therefore, the entire sample spot can be covered by a laser beam during laser irradiation The problem resulting from inhomogeneous sample deposition that can cause poor shot-to-shot reproducibility can be eliminated. Reliable quantitative MS results with good reproducibility may be obtained.

References

1. Karas M, Bachmann D, Hillenkamp F. 1985 Influence of the wavelength in high-irradiance ultraviolet laser desorption mass spectrometry of organic molecules. *Anal. Chem.* **57**, 2935–2939. (doi:10.1021/ac00291a042)

2. Karas M, Hillenkamp F. 1988 Laser desorption ionization of proteins with molecular masses exceeding 10 000 daltons. *Anal. Chem.* **60**, 2299–2301. (doi:10.1021/ac00171a028)

3. Tanaka K, Waki H, Ido Y, Akita S, Yoshida Y, Yoshida T, Matsuo T. 1988 Protein and polymer analyses up to *m/z* 100 000 by laser ionization time-of flight mass spectrometry. *Rapid Commun. Mass Spectrom.* **2**, 151–153. (doi:10.1002/rcm.1290020802)

4. Sunner J, Dratz E, Chen Y-C. 1995 Graphite surface-assisted laser desorption/ionization time-of-flight mass spectrometry of peptides and proteins from liquid solutions. *Anal. Chem.* **67**, 4335–4342. (doi:10.1021/ac00119a021)

5. Chen YC, Shiea J, Sunner J. 1998 Thin-layer chromatography-mass spectrometry using activated carbon, surface-assisted laser desorption/ionization. *J. Chromatogr. A* **826**, 77–86. (doi:10.1016/S0021-9673(98)00726-2)

6. Chen Y-C, Tsai M-F. 2000 Using surfactants to enhance the analyte signals in activated carbon, surface-assisted laser desorption/ionization (SALDI) mass spectrometry. *J. Mass Spectrom.* **35**, 1278–1284. (doi:10.1002/1096-9888(200011)35)

7. Chen Y-C, Tsai M-F. 2000 Sensitivity enhancement for nitrophenols using cationic surfactant-modified activated carbon for solid-phase extraction surface-assisted laser desorption/ionization mass spectrometry. *Rapid Commun. Mass Spectrom.* **14**, 2300–2304. (doi:10.1002/1097-0231(20001215)14)

8. Wei J, Buriak JM, Siuzdak G. 1999 Desorption-ionization mass spectrometry on porous silicon. *Nature* **399**, 243–246. (doi:10.1038/20400)

9. Lin Y-S, Chen Y-C. 2002 Laser desorption/ionization time-of-flight mass spectrometry on sol-gel-derived 2,5-dihydroxybenzoic acid film. *Anal. Chem.* **74**, 5793–5798. (doi:10.1021/ac020418a)

10. Chen C-T, Chen Y-C. 2005 Fe_3O_4/TiO_2 core/shell nanoparticles as affinity probes for the analysis of phosphopeptides using TiO_2 surface-assisted laser desorption/ionization mass spectrometry. *Anal. Chem.* **77**, 5912–5919. (doi:10.1021/ac050831t)

11. Chen W-Y, Chen Y-C. 2006 Affinity based mass spectrometry by using iron oxide magnetic particles as the matrix and concentrating probes for SALDI MS analysis of peptides and proteins. *Anal. Bioanal. Chem.* **386**, 699–704. (doi:10.1007/s00216-006-0427-0)

12. Dattelbaum AM, Iyer S. 2006 Surface-assisted laser desorption/ionization mass spectrometry. *Expert Rev. Proteomics* **3**, 153–161. (doi:10.1586/14789450.3.1.153)

13. Lo C-Y, Lin J-Y, Chen W-Y, Chen C-T, Chen Y-C. 2008 Surface-assisted laser desorption/ionization mass spectrometry on titania nanotube arrays. *J. Am. Soc. Mass Spectrom.* **19**, 1014–1020. (doi:10.1016/j.jasms.2008.04.025)

14. Arakawa R, Kawasaki H. 2010 Functionalized nanoparticles and nanostructured surfaces for surface-assisted laser desorption/ionization mass spectrometry. *Anal. Sci.* **26**, 1229–1240. (doi:org/10.2116/analsci.26.1229)

15. Chiang C-K, Chen W-T, Chang H-T. 2011 Nanoparticle-based mass spectrometry for the analysis of biomolecules. *Chem. Soc. Rev.* **40**, 1269–1281. (doi:10.1039/c0cs00050g)

16. Amini N, Shariatgorji M, Thorsén G. 2009 SALDI-MS signal enhancement using oxidized graphitized carbon black nanoparticles. *J. Am. Soc. Mass Spectrom.* **20**, 1207–1213. (doi:10.1016/j.jasms.2009.02.017)

17. Hsu WY, Lin WD, Hwu WL, Lai CC, Tsai FJ. 2010 Screening assay of very long chain fatty acids in human plasma with multiwalled carbon nanotube-based surface-assisted laser desorption/ionization mass spectrometry. *Anal. Chem.* **82**, 6814–6820. (doi:10.1021/ac100772j)

18. Lin Z, Zheng J, Lin G, Tang Z, Yang X, Cai Z. 2015 Negative ion laser desorption/ionization time-of-flight mass spectrometric analysis of small molecules using graphitic carbon nitride nanosheet matrix. *Anal. Chem.* **87**, 8005–8012. (doi:10.1021/acs.analchem.5b02066)

19. Su CL, Tseng WL. 2007 Gold nanoparticles as assisted matrix for determining neutral small carbohydrates through laser desorption/ionization time-of-flight mass spectrometry. *Anal. Chem.* **79**, 1626–1633. (doi:10.1021/ac061747w)

20. Chiang C-K, Lin Y-W, Chen W-T, Chang H-T. 2010 Accurate quantitation of glutathione in cell lysates through surface-assisted laser desorption/ionization mass spectrometry using gold nanoparticles. *Nanomedicine* **6**, 530–537. (doi:10.1016/j.nano.2010.01.006)

21. Chen W-T, Chiang C-K, Lin Y-W, Chang H-T. 2010 Quantification of captopril in urine through surface-assisted laser desorption/ionization mass spectrometry using 4-mercaptobenzoic acid-capped gold nanoparticles as an internal standard. *J. Am. Soc. Mass Spectrom.* **21**, 864–867. (doi:10.1016/j.jasms.2010.01.023)

22. Kuo T-R, Chen J-S, Chiu Y-C, Tsai C-Y, Hu C-C, Chen C-C. 2011 Quantitative analysis of multiple urinary biomarkers of carcinoid tumors through gold-nanoparticle-assisted laser desorption/ionization time-of-flight mass spectrometry. *Anal. Chim. Acta* **699**, 81–86. (doi:10.1016/j.aca.2011.05.012)

23. Kailasa SK, Wu HF. 2012 One-pot synthesis of dopamine dithiocarbamate functionalized gold nanoparticles for quantitative analysis of small molecules and phosphopeptides in SALDI- and MALDI-MS. *Analyst* **137**, 1629–1638. (doi:10.1039/c2an16008k)

24. Chiu WC, Huang CC. 2013 Combining fibrinogen-conjugated gold nanoparticles with a cellulose membrane for the mass spectrometry-based detection of fibrinolytic-related proteins. *Anal. Chem.* **85**, 6922–6929. (doi:10.1021/ac4013418)

25. Chiu T-C, Chang L-C, Chiang C-K, Chang H-T. 2008 Determining estrogens using surface-assisted laser desorption/ionization mass spectrometry with silver nanoparticles as the matrix. *J. Am. Soc. Mass Spectrom.* **19**, 1343–1346. (doi:10.1016/j.jasms.2008.06.006)

26. Shrivas K, Wu HF. 2008 Applications of silver nanoparticles capped with different functional groups as the matrix and affinity probes in surface-assisted laser desorption/ionization time-of-flight and atmospheric pressure matrix-assisted laser desorption/ionization ion trap mass spectrometry for rapid analysis of sulfur drugs and biothiols in human urine. *Rapid Commun. Mass Spectrom.* **22**, 2863–2872. (doi:10.1002/rcm.3681)

27. Iwaki Y, Kawasaki H, Arakawa R. 2012 Human serum albumin-modified Fe3O4 magnetic nanoparticles for affinity-SALDI-MS of small-molecule drugs in biological liquids. *Anal. Sci.* **28**, 893–900. (doi:10.2116/analsci.28.893)

28. Osaka I, Okumura K, Miyake N, Watanabe T, Nozaki K, Kawasaki H, Arakawa R. 2010 Quantitative analysis of an antioxidant additive in soluble plastics by surface-assisted laser desorption/ionization mass spectrometry (SALDI-MS) using TiO$_2$ nanoparticles. *J. Mass Spectrom. Soc. Jpn.* **58**, 123–127. (doi:10.5702/massspec.58.123)

29. Chiu T-C. 2011 Steroid hormones analysis with surface-assisted laser desorption/ionization mass spectrometry using catechin-modified titanium dioxide nanoparticles. *Talanta* **86**, 415–420. (doi:10.1016/j.talanta.2011.09.038)

30. Shrivas K, Hayasaka T, Sugiura Y, Setou M. 2011 Method for simultaneous imaging of endogenous low molecular weight metabolites in mouse brain using TiO$_2$ nanoparticles in nanoparticle-assisted laser desorption/ionization-imaging mass spectrometry. *Anal. Chem.* **83**, 7283–7289. (doi:10.1021/ac201602s)

31. Lee K-H, Chiang C-K, Lin Z-H, Chang H-T. 2007 Determining enediol compounds in tea using surface-assisted laser desorption/ionization mass spectrometry with titanium dioxide nanoparticle matrices. *Rapid Commun. Mass Spectrom.* **21**, 2023–2030. (doi:10.1002/rcm.3058)

32. Huang MF, Chang HT. 2012 Detection of carbohydrates using surface-assisted laser desorption/ionization mass spectrometry with HgTe nanostructures. *Chem. Sci.* **3**, 2147–2152. (doi:10.1039/C2SC01066F)

33. Kailasa SK, Kiran K, Wu HF. 2008 Comparison of ZnS semiconductor nanoparticles capped with various functional groups as the matrix and affinity probes for rapid analysis of cyclodextrins and proteins in surface-assisted laser desorption/ionization time-of-flight mass spectrometry. *Anal. Chem.* **80**, 9681–9688. (doi:10.1021/ac8015664)

34. Alhmoud HZ, Guinan TM, Elnathan R, Kobus H, Voelcker NH. 2014 Surface-assisted laser desorption/ionization mass spectrometry using ordered silicon nanopillar arrays. *Analyst* **139**, 5999–6009. (doi:10.1039/c4an01391c)

35. Guinan T, Ronci M, Vasani R, Kobus H, Voelcker NH. 2015 Comparison of the performance of different silicon-based SALDI substrates for illicit drug detection. *Talanta* **132**, 494–502. (doi:10.1016/j.talanta.2014.09.040)
36. López de Laorden C, Beloqui A, Yate L, Calvo J, Puigivila M, Llop J, Reichardt NC. 2015 Nanostructured indium tin oxide slides for small-molecule profiling and imaging mass spectrometry of metabolites by surface-assisted laser desorption ionization MS. *Anal. Chem.* **87**, 431–440. (doi:10.1021/ac5025864)
37. Hu J-B, Chen Y-C, Urban PL. 2013 Coffee-ring effects in laser desorption/ionization mass spectrometry. *Anal. Chim. Acta* **766**, 77–82. (doi:10.1016/j.aca.2012.12.044)
38. Yunker PJ, Still T, Lohr MA, Yodh AG. 2011 Suppression of the coffee-ring effect by shape-dependent capillary interactions. *Nature* **476**, 308–311. (doi:10.1038/nature10344)
39. Lai H-Z, Wang S-G, Wu C-Y, Chen Y-C. 2015 Detection of *Staphylococcus aureus* by functional gold nanoparticle-based affinity surface-assisted laser desorption/ionization mass spectrometry. *Anal. Chem.* **87**, 2114–2120. (doi:10.1021/ac503097v)
40. Chen X, Mao SS. 2007 Titanium dioxide nanomaterials: synthesis, properties, modifications, and applications. *Chem. Rev.* **107**, 2891–2959. (doi:10.1021/cr0500535)
41. Du YL, Deng Y, Zhang MS. 2006 Variable-temperature Raman scattering study on anatase titanium dioxide nanocrystals. *J. Phys. Chem. Solids* **67**, 2405–2408. (doi:10.1016/j.jpcs.2006.06.020)
42. Urban PL, Jefimovs K, Amantonico A, Fagerer SR, Schmid T, Mädler S, Puigmarti-Luis J, Goedecke N, Zenobi R. 2010 High-density micro-arrays for mass spectrometry. *Lab Chip* **10**, 3206–3209. (doi:10.1039/c0lc00211a)